How to cite: *Angew. Chem. Int. Ed.* **2021**, *60*, 27039–27045
International Edition: doi.org/10.1002/anie.202111939
German Edition: doi.org/10.1002/ange.202111939

Redox Flow Batteries

Development of High Energy Density Diaminocyclopropenium-Phenothiazine Hybrid Catholytes for Non-Aqueous Redox Flow Batteries

*Yichao Yan, David B. Vogt, Thomas P. Vaid, Matthew S. Sigman, and Melanie S. Sanford**

Abstract: *This report describes the design of diaminocyclopropenium-phenothiazine hybrid catholytes for non-aqueous redox flow batteries. The molecules are synthesized in a rapid and modular fashion by appending a diaminocyclopropenium (DAC) substituent to the nitrogen of the phenothiazine. Combining a versatile C-N coupling protocol (which provides access to diverse derivatives) with computation and structure-property analysis enabled the identification of a catholyte that displays stable two-electron cycling at potentials of 0.64 and 1.00 V vs. Fc/Fc^+ as well as high solubility in all oxidation states ($\geq$ 0.45 M in $TBAPF_6$/MeCN). This catholyte was deployed in a high energy density two-electron RFB, exhibiting >90% capacity retention over 266 hours of flow cell cycling at >0.5 M electron concentration.*

Introduction

Nonaqueous redox flow batteries (RFBs) offer opportunities for achieving high energy density storage due to the large electrochemical potential window of organic solvents.[1,2] To take complete advantage of this large potential window, it is critical to develop storage materials (catholytes and anolytes) that undergo multiple reversible redox reactions at extreme potentials, exhibit high solubility in all oxidation states, and possess high calendar and cycling stability.[3–20] Over the past decade, a variety of anolytes that fit these criteria have been identified.[16,21–25] In marked contrast, their multi-electron catholyte counterparts remain extremely limited.[3–20] Phenothiazine is a rare example of a catholyte that undergoes two reversible electron transfers in organic solvents.[7,11,15,26–28] However, as depicted in Figure 1, existing phenothiazine derivatives suffer from some combination of modest solubility, modest oxidation potential, and/or poor electrochemical stability for the second couple.[7,11,15,28]

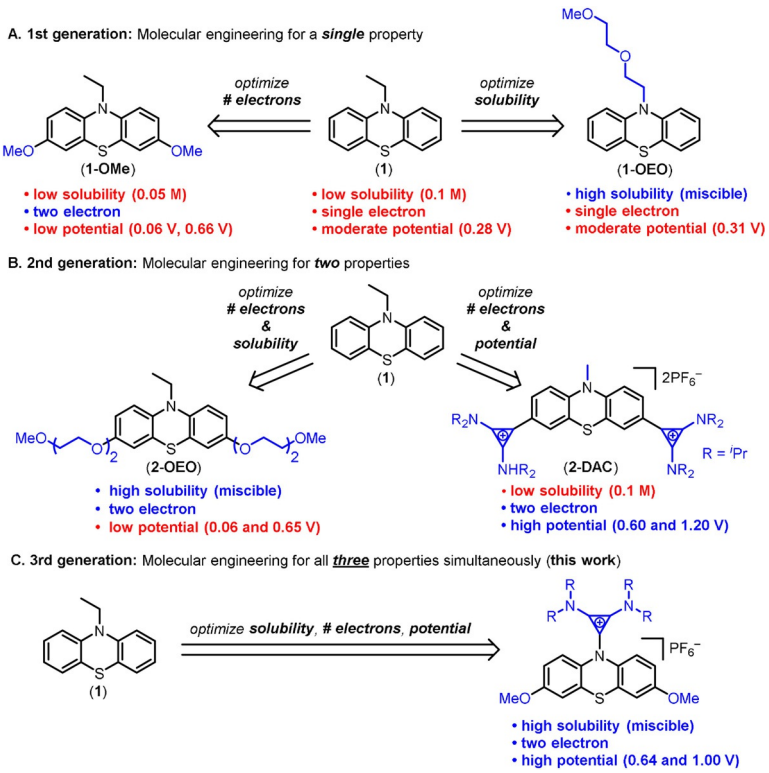

Figure 1. Evolution of phenothiazine-based catholytes.

Several research teams have made progress in the molecular engineering of next-generation phenothiazine derivatives (Figure 1).[11,26,28–32] Odom and co-workers conducted early investigations of the parent *N*-ethyl phenothiazine (**1**) and disclosed that it suffers from low solubility (0.1 M for the neutral molecule and 0.1 M for the radical cation in $TEABF_4$/MeCN) and an unstable second oxidation.[26] As shown in Figure 1A, their team initially used molecular engineering to address each of these individual properties. For instance, they showed that replacing the *N*-ethyl substituent with an *N*-oligoethylene oxide (OEO) chain (**1-OEO**) resulted in dramatically enhanced solubility for both the neutral (miscible) and radical cation (0.5 M) in $TEABF_4$/MeCN. However, the second oxidative couple of **1-OEO**

[*] Y. Yan, Dr. T. P. Vaid, Prof. M. S. Sanford
Department of Chemistry, University of Michigan
930 North University Avenue, Ann Arbor, MI 48109 (USA)
E-mail: mssanfor@umich.edu
Dr. D. B. Vogt, Prof. M. S. Sigman
Department of Chemistry, University of Utah
315 South 1400 East, Salt Lake City, UT 84112 (USA)
Y. Yan, Dr. D. B. Vogt, Dr. T. P. Vaid, Prof. M. S. Sigman, Prof. M. S. Sanford
Joint Center for Energy Storage Research (JCESR)
9700 South Cass Avenue, Argonne, IL 60439 (USA)
Supporting information and the ORCID identification number(s) for the author(s) of this article can be found under: https://doi.org/10.1002/anie.202111939.

remained unstable, so only single-electron cycling could be achieved.[26] In a separate study, Odom and co-workers demonstrated that stable two-electron cycling could be realized by installing electron-donating methoxy (MeO-) substituents at the 3- and 7- sites of the phenothiazine core (**1-OMe**). However, this resulted in a significant ($\approx$300 mV) decrease in the redox potential for each couple.[11,28] In addition, the solubility of **1-OMe** is poor (0.05 M in 0.5 M TEATFSI/MeCN).

Second-generation approaches have leveraged these early insights to simultaneously optimize two properties of phenothiazines (Figure 1B). For instance, Odom and co-workers demonstrated that integrating oligoethylene oxide groups at the 3- and 7-sites (**2-OEO**) results in enhanced solubility (miscible) as well as stable two-electron cycling, albeit at low potentials (0.06 and 0.65 V vs. Fc/Fc$^+$).[28] Additionally, our group recently showed that installing resonance electron-withdrawing diaminocyclopropenium substituents at the 3- and 7- positions (**2-DAC**) results in both stabilization of the second redox couple and an $\approx$600 mV increase in redox potential relative to **1-OMe** (to 0.6 and 1.2 V).[33] However, **2-DAC** remains limited by extremely poor solubility in the electrolyte solution (0.09 M in MeCN). Additionally, **2-DAC** derivatives bearing different substituents are not readily accessible due to challenges associated with the C–C bond-forming step that couples the DAC to the phenothiazine core.

In this report, we identify next generation diaminocyclopropenium-phenothiazine hybrid catholytes of the general structure **3** that can be synthesized in a rapid and modular fashion, thus expediting molecular engineering of all three key properties simultaneously (Figure 1C). We demonstrate that attaching the DAC to phenothiazine via a C–N bond (rather than a C–C bond) circumvents the synthetic challenges associated with **2-DAC**. Combining this modular C-N coupling protocol with computation and structure-property analysis enabled the identification of a derivative that displays stable two-electron cycling at high potentials (0.64 and 1.00 V vs. Fc/Fc$^+$) as well as high solubility ($\geq$0.45 M in TBAPF$_6$/MeCN in all relevant redox states). This catholyte was deployed in a two-electron RFB, exhibiting $>$90% capacity retention over 266 hours of flow cell cycling at $>$0.5 M electron concentration.

Results and Discussion

As discussed above, appending diaminocyclopropenium substituents onto the phenothiazine core (**2-DAC**) results in a dramatic increase in redox potential as well as stabilization of two-electron cycling compared to the parent catholyte **1**.[33] However, **2-DAC** displays poor solubility in MeCN and has an undesirably high molecular weight ($\approx$1000 g mol^{-1}), which limits the maximum achievable concentration in an RFB.[34] Literature precedent suggests that modifying the DAC substituents could be effective for enhancing solubility.[35,36] However, many analogues of **2-DAC** bearing different R groups were not synthetically available because the C–C coupling of the phenothiazine with the cyclopropenium requires bulky diisopropylamino groups in order to limit side reactions. Additionally, the original scaffold design and synthetic approach does not accommodate diverse substituents on the phenothiazine core.

We reasoned that these challenges could be addressed by changing the attachment linkage between the two components. Specifically, we hypothesized that diverse DAC and phenothiazine derivatives could be coupled in a single synthetic step via a carbon-nitrogen bond-forming reaction between the parent phenothiazine and 1-chloro-2,3-bis(dialkylamino)cyclopropenium chlorides.[37,38] Diverse substitution can be incorporated on both reaction partners, enabling the one-step synthesis of 10 derivatives (Scheme 1, series **3** and **4**). All products were characterized via ^{1}H and ^{13}C NMR spectroscopy as well as high resolution mass spectrometry.

The redox properties of the catholyte candidates in series **3** and **4** were initially interrogated using cyclic voltammetry (CV). CV experiments were conducted using 5 mM solutions of the redox active molecules in 0.5 M TBAPF$_6$/MeCN with a glassy carbon working electrode (0.071 cm^2, BASi) and a scan rate of 100 mV s^{-1}. Representative CVs are shown in Figure 2, and the redox potential (vs. Fc/Fc$^+$) and peak height ratio for each couple are summarized in Table 1.

The phenothiazine-derived compound **3-^{i}Pr** undergoes two single-electron oxidations at 0.70 and $\approx$1.40 V vs. Fc/Fc$^+$. Notably, these oxidation potentials are 100–200 mV higher than those of **2-DAC** (0.60 and 1.20 V vs. Fc/Fc$^+$), despite the presence of a single DAC moiety on **3-^{i}Pr**. However, unlike **2-DAC**, the second oxidation is not reversible, as indicated by

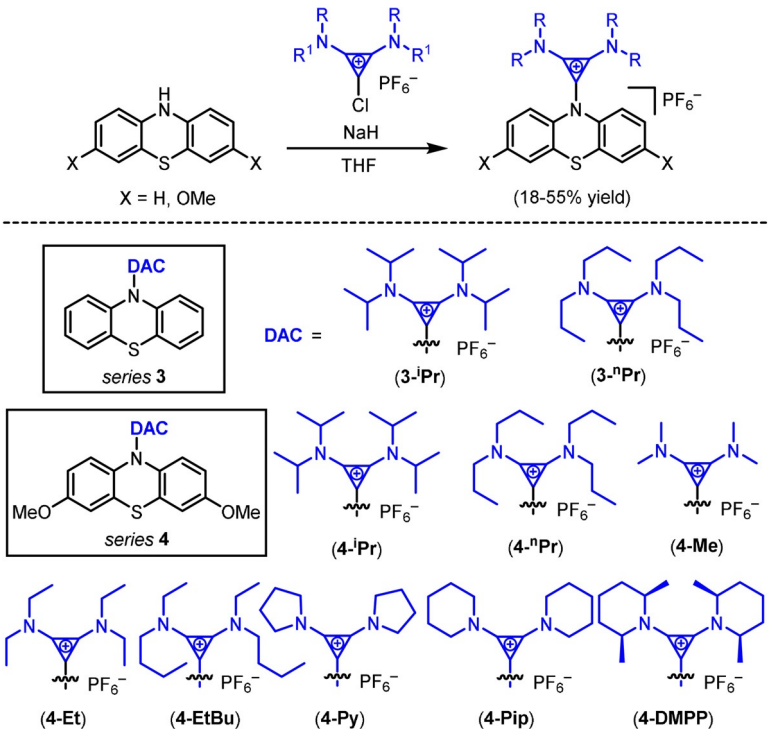

Scheme 1. Synthesis of **3** and **4**.

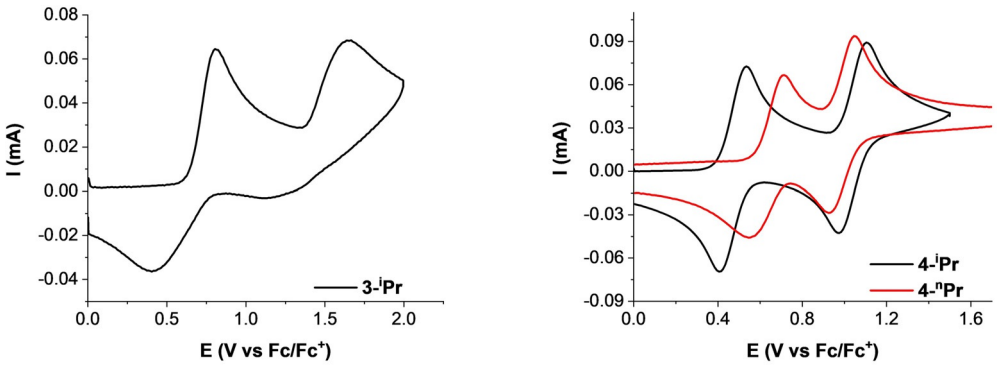

Figure 2. Left: CV of **3-^{i}Pr**. Right: CVs of **4-^{i}Pr** (black) and **4-^{n}Pr** (red). CVs conducted with 5 mM solutions of the redox active molecules in 0.5 M $TBAPF_6$ in MeCN at 100 mVs^{-1} scan rate.

Table 1: CV data of all compounds.

compound	1st $E_{1/2}$[a]	i_{pc1}/i_{pa1}[b]	2nd $E_{1/2}$[a]	i_{pc2}/i_{pa2}[b]
3-^{i}Pr	0.70 V	0.93	1.40 V	irreversible
3-^{n}Pr	0.72 V	0.90	1.30 V	0.83
4-^{i}Pr	0.47 V	1.00	1.04 V	0.97
4-^{n}Pr	0.67 V	0.99	1.00 V	1.02
4-Me	0.65 V	0.97	1.01 V	1.02
4-Et	0.65 V	0.92	1.00 V	1.01
4-EtBu	0.65 V	0.92	1.00 V	1.07
4-Py	0.65 V	0.96	0.95 V	1.07
4-Pip	0.63 V	0.97	1.00 V	1.03
4-DMPP	0.64 V	0.93	1.00 V	1.05

[a] 2.5 mM substrate in 0.5 M TBAPF6/MeCN and referenced to Fc/Fc^{+}. [b] Calculated at a scan rate of 20 mVs^{-1}.

the lack of a significant return wave for this peak (Figure 2 left). In addition, **3-^{i}Pr** exhibits only modest (0.15 M) solubility in 0.5 M $TBAPF_6$/MeCN. The *n*-propyl derivative **3-^{n}Pr** undergoes oxidation at slightly higher potentials (0.72 and 1.30 V vs. Fc/Fc^{+}) but also exhibits low stability in the second redox couple ($i_{pc2}/i_{pa2} = 0.83$, see Figure S2 for multiple CV scans of **3-^{n}Pr**). However, the solubility of **3-^{n}Pr** is more than five-fold higher than that of **3-^{i}Pr** (0.86 in 0.5 M $TBAPF_6$/MeCN), indicating that modification of the DAC substituents is an effective approach to tuning solubility in these systems.

On the basis of Odom's previous work,[27] we reasoned that the reversibility of the second redox couple could be enhanced by introducing methoxy (MeO-) substituents at the 3- and 7-positions of the phenothiazine core. To test this hypothesis, we synthesized and evaluated **4-iPr**. As illustrated in Figure 2 right, the CV of **4-iPr** displays two single-electron oxidations at 0.47 V and 1.04 vs. Fc/Fc^{+}. While these potentials are 200–400 mV lower than those of **3-iPr**, the second oxidation exhibits significantly enhanced reversibility versus that of **3-iPr** ($i_{pc2}/i_{pa2} = 0.97$ at a scan rate of 100 mVs^{-1} for the oxidation at 1.04 V in **4-iPr**).

We next changed the amine substituent from isopropyl to *n*-propyl with the goal of improving the solubility of **4-^{i}Pr** (which is just 0.08 M in 0.5 M $TBAPF_6$/MeCN). Indeed, **4-^{n}Pr** exhibits > 15-fold higher solubility than **4-^{i}Pr** (1.42 M in 0.5 M $TBAPF_6$/MeCN). Unexpectedly, the oxidation potential also changes significantly between the *iso*-propyl and *n*-propyl derivatives. While the second oxidation occurs at comparable potential ($E_{1/2} = 1.00$ V for **4-^{n}Pr** and 1.06 V for **4-^{i}Pr**), the first oxidation for **4-^{n}Pr** is almost 200 mV higher ($E_{1/2} = 0.65$ V versus 0.47 V, respectively).[36]

To identify trends in this first oxidation potential as a function of DAC nitrogen substituent, we explored a series of derivatives bearing methyl (**4-Me**), ethyl (**4-Et**), ethyl butyl (**4-EtBu**), pyrrolidine (**4-Py**), piperidine (**4-Pip**), and 2,6-dimethylpiperidine (**4-DMPP**) substituents. As summarized in Table 1 and Figure 2, these derivatives all show two reversible oxidations with peak height ratios close to 1. Furthermore, their oxidation potentials are all nearly identical to those of **4-^{n}Pr**. Thus, rather than a trend of potential as a function of nitrogen substituent, we see that **4-^{i}Pr** is the only molecule with a lower first redox potential.

To investigate the origin of this outcome, we turned to computational analysis via density-functional theory (DFT; see Supporting Information for complete details). We hypothesized that oxidation potential in these systems is influenced by overlap between the electron-poor cyclopropenium and electron-rich phenothiazine orbitals, which affects the overall charge distribution in the molecule. To evaluate this proposal, we collected Boltzmann-averaged data from a conformational ensemble of each molecule in series **4** (Table 1). We collected these data for both the unoxidized molecule (+1 charge, **4**) and the two oxidation products [+2 charge ($\mathbf{4}^{\bullet+}$) and +3 charge ($\mathbf{4}^{++}$)].

These studies reveal that the steric bulk of **4-^{i}Pr** imposes a drastic geometric change that accompanies removal of the first electron (ΔDAC^{+} $twist_{(ox1)} = 71°$, Figure 3 A) and ultimately results in nearly perpendicular ($DAC^{\bullet+}$ twist = 87°), and thus unconjugated, ring systems in the first oxidation product **4-^{i}Pr$^{\bullet+}$**. In contrast, this geometric change is much less pronounced in the other series **4** electrolytes (average $\Delta DAC^{\bullet+}$ $twist_{(ox1)} = 29 \pm 0.6°$ for all series **4** compounds excluding **4-^{i}Pr**, Figure 3 A, **4-Me** shown as representative example), thus yielding a more conjugated first oxidation product ($DAC^{\bullet+}$ twist = 46° for **4-Me$^{\bullet+}$**). This effect can also be seen in Figure 3 B when comparing the singly occupied molecular orbital (SOMO) of the first oxidation products, **4-^{i}Pr$^{\bullet+}$** and **4-Me$^{\bullet+}$**.

Overall, this analysis indicates that the first oxidation of **4-^{i}Pr** is effectively isolated to the dimethoxyphenothiazine core, with the DAC substituent serving as an inductive electron withdrawing group. This results in a positive shift in potential relative to that of the parent **1-OMe** (from 0.06 V to 0.47 V vs. Fc/Fc^{+}). In contrast, the first oxidation of **4-Me** occurs across both rings, and thus can be viewed as a mixture of the two component redox potentials, resulting in a significantly more positive first oxidation potential (at 0.65 V vs. Fc/Fc^{+}).

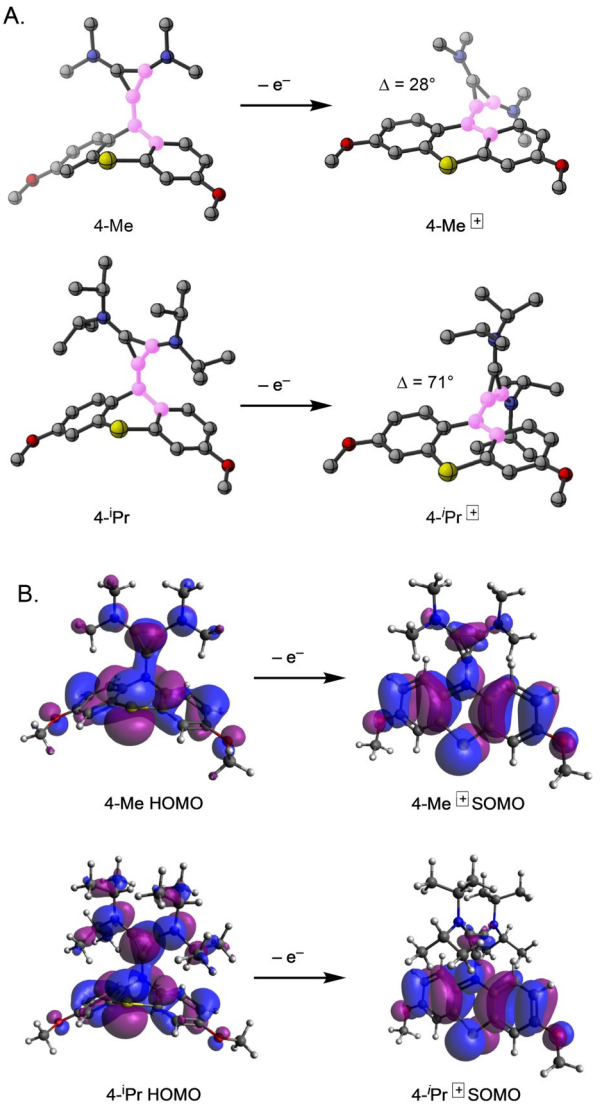

Figure 3. A) Geometry changes accompanying the first oxidation of **4-Me** (used as a representative example of the series **4** compounds; data for the other series **4** molecules is in the Supporting Information) and **4-^{i}Pr**. "DAC $^{+}$ twist" is visualized by the dihedral angle highlighted in pink. B) HOMO and SOMO of **4-Me** and **4-^{i}Pr** before (+1 charge) and after the first oxidation (+2 charge).

While the first oxidation of **4-^{i}Pr** occurs at lower potential than that of the other series **4** derivatives in Table 1, the second oxidation is at nearly the same potential ($\approx$1.0 V) for all eight compounds. We evaluated the geometries and frontier molecular orbitals of the second oxidation products ($\mathbf{4}^{++}$) and found a uniformly insignificant amount of geometric reorganization accompanying the removal of the second electron (average ΔDAC$^{\bullet+}$ twist$_{(ox2)}$ = 12 $\pm$ 8° for all series 4 compounds). Additionally, for both **4-^{i}Pr$^{\bullet+}$** and **4-Me$^{\bullet+}$**, the majority of SOMO electron density is concentrated on the phenothiazine portion of the molecule despite **4-^{i}Pr** having less conjugation between the rings (Figure 3 B, **4-^{i}Pr$^{\bullet+}$** and **4-Me$^{\bullet+}$** SOMO). This suggests that conjugation between the two rings plays a minimal role in the second oxidation. Thus, the large difference in DAC$^{\bullet+}$ twist angle between the two structures (which is maintained in **4-^{i}Pr^{++}** and **4-Me^{++}**, see Supporting information for complete details) does not manifest in significantly different potentials for this second oxidation.

We next compared capacity retention in series **4** derivatives during charge-discharge cycling in a static H-cell. These experiments were conducted in a three-electrode H-cell separated with an ultrafine glass frit, using reticulated vitreous carbon (RVC) working and counter electrodes.[35] Two-electron cycling was conducted with a 2.5 mM solution of **4** in 0.5 M $TBAPF_6$/acetonitrile on both the working and counter electrode sides of the cell. After the initial charge, the solution on the counter electrode side was exchanged for a fresh solution of **4** in 0.5 M $TBAPF_6$/acetonitrile to enable symmetrical two-electron cycling. The solution on the working side of the cell was charged at a rate of 2.5 C using voltaic cutoffs to achieve the maximum state-of-charge (SOC). The discharged capacity was then monitored versus cycle number to assess capacity retention. As summarized in Table 2, over 100 cycles all eight of these derivatives show comparable capacity fade (14–31 %) and coulombic efficiency (98–99 %) while charging similar amounts of catholyte during cycling (achieving 78–87 % of theoretical capacity).

Table 2: Capacity retention data for the two-electron cycling of **4** in an H-cell.

compound	accessed capacity[a] [%]	coulombic efficiency [%]	capacity fade in 100 cycles [%]
4-Me	77.7	>98	28.7
4-Et	80.0	>98	21.2
4-^{n}Pr	81.7	>98	31.7
4-^{i}Pr	78.3	>99	14.9
4-EtBu	84.8	>99	13.8
4-Py	86.5	>99	17.5
4-Pip	85.8	>99	15.2
4-DMPP	81.9	>99	14.5

[a] 2.5 mM substrate in 0.5 M $TBAPF_6$/MeCN.

Based on the similar charge-discharge cycling data for the compounds in series **4**, we moved forward with the most soluble of these derivatives for flow cell cycling. While **4-Me**, **4-Et**, **4-^{n}Pr**, **4-^{i}Pr**, **4-pip**, and **4-py** are solids at room temperature, **4-EtBu** and **4-DMPP** are viscous oils that are fully miscible in 0.5 M $TBAPF_6$/MeCN. Thus, each of these two-electron catholytes was next cycled in a flow cell, using viologen **5** (see Figure 4) as a two-electron anolyte.[22,23,39,40] The flow cell contains graphite charge collecting plates with an interdigitated flow field in combination with 400 µm thick carbon-felt electrodes. The electrolyte solutions were flowed through the cell at 10 mL min^{-1} and were subjected to galvanostatic cycling at 40 mA cm^{-2}. The cell was separated by a Celgard 4560 membrane. For initial cycling studies, the catholyte and anolyte reservoirs were loaded with identical solutions containing 50 mM of **4-EtBu** or **4-DMPP** and 50 mM of **5** in 0.50 M MeCN/$TBAPF_6$. In these systems, the electron concentration is 0.1 M, with a battery potential up to 2.2 V, and a theoretical capacity of 2.68 Ah L^{-1}.

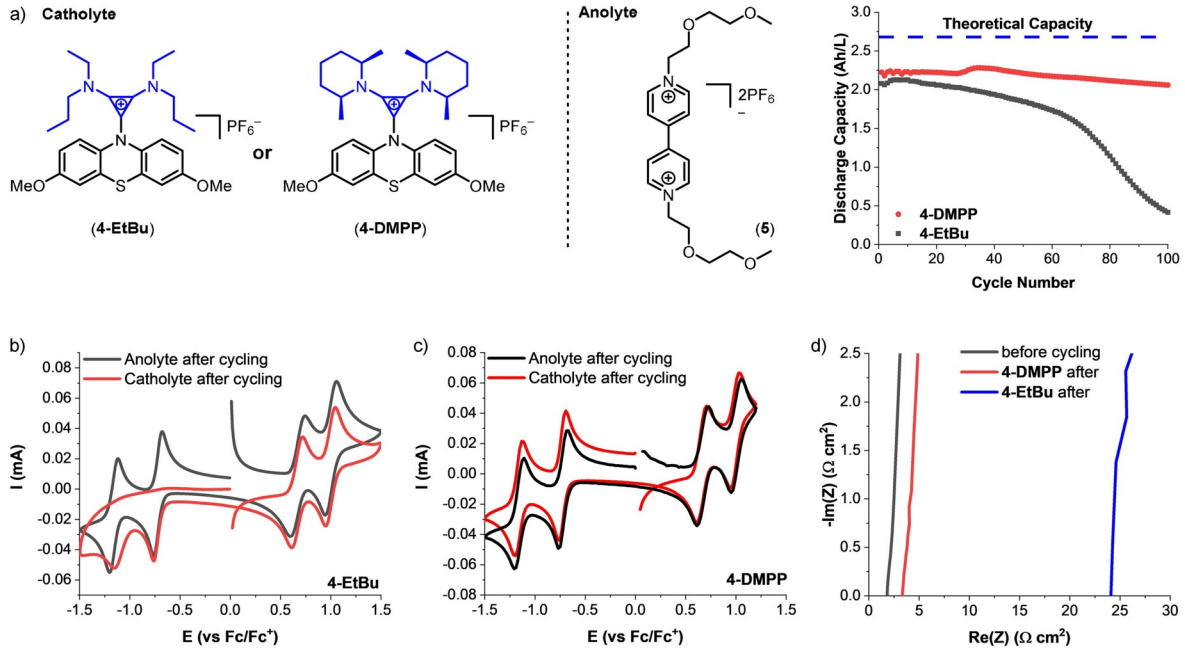

Figure 4. a) Flow cell cycling of 50 mM **4-DMPP** or **4-EtBu** as catholyte and 50 mM **5** as anolyte. b) CVs after flow cell cycling of **4-EtBu** (black = anolyte side of cell; red = catholyte side of cell). c) CVs after flow cell cycling of **4-DMPP** (black = anolyte side of cell; red = catholyte side of cell); d) Electrochemical impedance spectroscopy (EIS) on cells for before and after 100 cycles.

Figure 4 shows the capacity retention data (panel a), pre- and post-cycling CVs (panels b and c), and pre- and post-cycling electrochemical impedance spectroscopy (EIS) measurements for the two flow cell experiments. The flow cells with **4-EtBu/5** and **4-DMPP/5** exhibit dramatically different performances, despite similar levels of material utilization (78 % and 85 %, respectively) and coulombic efficiency (91 % and 92 %, respectively) during cycling.[41] The **4-EtBu/5** flow cell shows much lower capacity retention over 100 cycles (20 % versus 91 % for **4-DMPP/5**). The post-cycling CV from the catholyte side of the **4-EtBu/5** cell (Figure 4b, red) shows that the reduction of **5** is no longer reversible. In addition, the post-cycling electrochemical impedance spectroscopy (EIS) of the **4-EtBu/5** cell shows an approximately 20-fold increase in the impedance. Collectively, these data suggest that decomposition of **4-EtBu** and **5** is occurring during flow cell cycling, likely depositing insoluble material on the electrodes and/or the membrane. The post-run CVs indicate that this is particularly problematic for the catholyte side of the cell, suggesting decomposition/side reactions between either **4-EtBu**$^{\cdot+}$ or **4-EtBu**$^{++}$ and the anolyte **5**. We also note that the cycling performance of **4-EtBu** is moderately improved when the experiment is conducted in the dark vs. in ambient light (34 % vs. 20 % capacity retention), suggesting that light plays a role in capacity fade in this system. This result is consistent with a recent report suggesting that *n*-alkyl substituted aminocyclopropenium derivatives are susceptible to light-mediated decomposition due to the accessibility of the α-protons.[42]

Based on the initial flow cell results, the **4-DMPP/5** system was selected for high concentration cycling. To assess the maximum feasible concentration for this battery, we evaluated solubility in the two limiting oxidation states: **4-DMPP** and **4-DMPP**$^{++}$ (the product of two-electron oxidation). **4-DMPP**$^{++}$ was prepared by bulk electrolysis (see Supporting Information for complete details).[35,38] The maximum solubilities of **4-DMPP** and **4-DMPP**$^{++}$ were then determined to be miscible and 0.45 M, respectively, in 0.5 M $TBAPF_6$/MeCN. Importantly, because **4-DMPP** undergoes two electron transfers, the limiting 0.45 M concentration of **4-DMPP**$^{++}$ corresponds to a 0.90 M electron concentration.

The mass transport and electrokinetics of **4-DMPP** were also evaluated. These properties are important for flow battery applications because fast diffusional and electron-transfer processes are critical for achieving high current densities and low overpotentials.[43] The diffusion coefficient was determined by varying the CV scan rate from 20 to 300 $mV\,s^{-1}$ and then applying the Randles-Sevcik equation (Figure S4). The observed values for **4-DMPP** (first couple: $5.77\times10^{-6}\,cm^2\,s^{-1}$; second couple: $4.51\times10^{-6}\,cm^2\,s^{-1}$) are comparable to those for other organic catholyte materials, including ferrocene derivative Fc1N112-TFSI ($4.25\times10^{-7}\,cm^2\,s^{-1}$)[44] and dialkoxybenzene derivative DBMMB ($5.77\times10^{-6}\,cm^2\,s^{-1}$),[45] as well as the related pheonthiazine derivatives **2-OEO** ($0.8\times10^{-6}\,cm^2\,s^{-1}$)[28] and **2-DAC** (first couple: $5.29\times10^{-6}\,cm^2\,s^{-1}$; second couple: $4.99\times10^{-6}\,cm^2\,s^{-1}$).[33] The heterogeneous electron-transfer rates were determined to be $4.84\times10^{-3}\,cm\,s^{-1}$ (first couple) and $4.62\times10^{-3}\,cm\,s^{-1}$ (second couple) using the Nicholson method (Figure S5).[46] Again, these are comparable to those for other catholyte materials, including 5,10-dihydro-5,10-dimethylphenazine ($5.53\times10^{-3}\,cm\,s^{-1}$),[7] $V(acac)_3$ ($6.5\times10^{-4}\,cm\,s^{-1}$),[43] and **2-DAC** (first couple: $2.53\times10^{-3}\,cm^2\,s^{-1}$; second couple: $3.47\times10^{-3}\,cm^2\,s^{-1}$).[33]

A high concentration flow cell was assembled using a mixture of **4-DMPP** (0.30 M in 0.50 M MeCN/$TBAPF_6$) and

5 (0.60 M in 0.50 M MeCN/TBAPF$_6$) as both the catholyte and anolyte.[47] For this experiment only the first reduction of **5** was accessed due to the modest solubility and stability of the doubly reduced viologen at high concentration. As such, the maximum cell potential in this system is 1.8 V. The charging and discharging rates were set to 60 mA cm^{-2}. These relatively fast rates are possible despite the high concentration due to the low resistance of the Daramic-175 membrane. The theoretical capacity of this system is 16.08 Ah L^{-1}, and the initial material utilization is 84%. As shown in Figure 5a, over 300 cycles (266 hours) 92.5% capacity retention was achieved with 89% coulombic efficiency and ≈70% energy efficiency, demonstrating the long-term cycling stability of **4-DMPP**.[48] Moreover, CVs of the diluted solution after cycling show no change in concentration of active species (Figure 5b). Instead, the observed capacity fade appears to be due to pressure/viscosity differences that result in preferential diffusion of the electrolyte solution to create a volume discrepancy in the reservoirs at the end of the experiment.

Conclusion

In summary, a novel soluble, high potential two-electron catholyte for non-aqueous RFBs has been developed. The discovery was enabled by linking phenothiazine to diaminocyclopropenium scaffolds via a C–N bond. The formation of this C–N bond is synthetically straightforward, thus facilitating the rapid, one-step synthesis of diverse derivatives and evaluation of the relationship between chemical structure and electrochemical and solubility properties. This enabled the simultaneous optimization of three key properties (solubility, two electron redox, and redox potential), resulting in a catholyte, **4-DMPP**, with one of the best combination of properties reported to date for this application (see Table S2 for a comparison of the redox potential, cycling stability, and discharge energy density of related systems). For instance, this molecule exhibits dramatically enhanced solubility and energy density relative to our previous generation of phenothiazine/diaminocyclopropenium hybrid catholyte **2-DAC**. In addition, the electrochemical cycling stability of **4-DMPP** far exceeds that of related high potential single electron catholytes, such as thiocyclopropenium derivatives (for comparison data, see Figure S9 and S10). Ultimately, we anticipate that this approach could prove generalizable to other catholyte candidates bearing amine and/or N-heterocyclic cores.

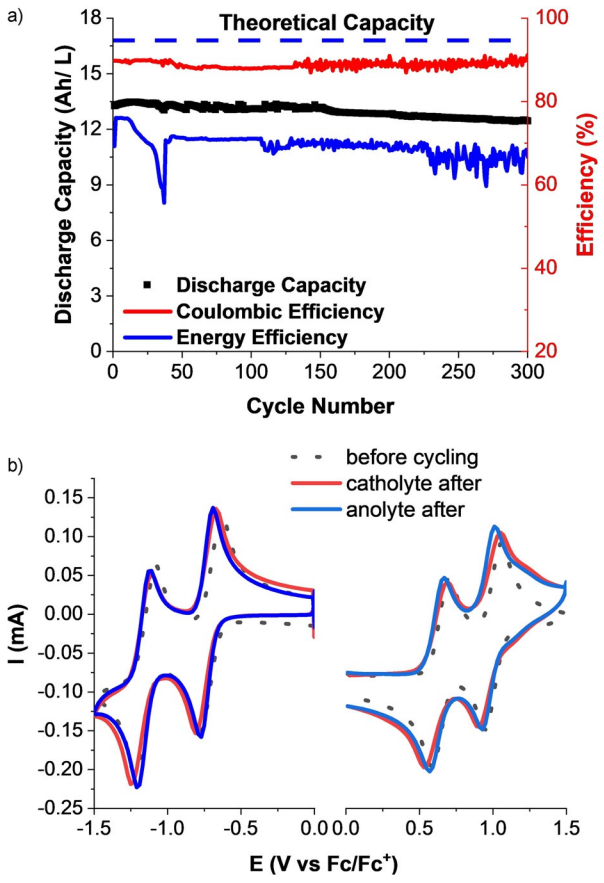

Figure 5. a) Flow cell cycling of 0.3 M of **4-DMPP** as catholyte and 0.6 M of **5** as anolyte. b) CV after cycling on both sides.

Acknowledgements

We thank Dr. Jeff W. Kampf for carrying out X-ray crystallographic analyses. This work was supported by the Joint Center for Energy Storage Research (JCESR) a Department of Energy, Energy Innovation Hub. Computational resources were provided from the Center for High Performance Computing (CHPC) at the University of Utah and the Extreme Science and Engineering Discovery Environment (XSEDE), which is supported by the National Science Foundation grant number ACI-1548562.

Conflict of Interest

The authors declare no conflict of interest.

Keywords: catholytes · cyclopropenium · organic redox flow batteries · phenothiazine

[1] J. Rugolo, M. J. Aziz, *Energy Environ. Sci.* **2012**, *5*, 7151–7160.
[2] C. J. Barnhart, M. Dale, A. R. Brandt, S. M. Benson, *Energy Environ. Sci.* **2013**, *6*, 2804–2810.
[3] X. Wei, W. Pan, W. Duan, A. Hollas, Z. Yang, B. Li, Z. Nie, J. Liu, D. Reed, W. Wang, V. Sprenkle, *ACS Energy Lett.* **2017**, *2*, 2187–2204.
[4] X. Wei, W. Xu, M. Vijayakumar, L. Cosimbescu, T. Liu, V. Sprenkle, W. Wang, *Adv. Mater.* **2014**, *26*, 7649–7653.
[5] J. Winsberg, T. Hagemann, S. Muench, C. Friebe, B. Häupler, T. Janoschka, S. Morgenstern, M. D. Hager, U. S. Schubert, *Chem. Mater.* **2016**, *28*, 3401–3405.
[6] C. Zhang, L. Zhang, Y. Ding, S. Peng, X. Guo, Y. Zhao, G. He, G. Yu, *Energy Storage Mater.* **2018**, *15*, 324–350.
[7] G. Kwon, S. Lee, J. Hwang, H.-S. Shim, B. Lee, M. H. Lee, Y. Ko, S.-K. Jung, K. Ku, J. Hong, K. Kang, *Joule* **2018**, *2*, 1771–1782.
[8] J. Zhang, Z. Yang, I. A. Shkrob, R. S. Assary, S. on Tung, B. Silcox, W. Duan, J. Zhang, C. C. Su, B. Hu, B. Pan, C. Liao, Z.

Zhang, W. Wang, L. A. Curtiss, L. T. Thompson, X. Wei, L. Zhang, *Adv. Energy Mater.* **2017**, *7*, 1701272.
[9] L. E. VanGelder, E. Schreiber, E. M. Matson, *J. Mater. Chem. A* **2019**, *7*, 4893 – 4902.
[10] L. E. VanGelder, A. M. Kosswattaarachchi, P. L. Forrestel, T. R. Cook, E. M. Matson, *Chem. Sci.* **2018**, *9*, 1692 – 1699.
[11] J. A. Kowalski, M. D. Casselman, A. Preet Kaur, J. D. Milshtein, C. F. Elliott, S. Modekrutti, N. Harsha Attanayake, N. Zhang, S. R. Parkin, C. Risko, F. R. Brushett, S. A. Odom, *J. Mater. Chem. A* **2017**, *5*, 24371 – 24379.
[12] I. L. Escalante-García, J. S. Wainright, L. T. Thompson, R. F. Savinell, *J. Electrochem. Soc.* **2015**, *162*, A363 – A372.
[13] E. V. Carino, J. Staszak-Jirkovsky, R. S. Assary, L. A. Curtiss, N. M. Markovic, F. R. Brushett, *Chem. Mater.* **2016**, *28*, 2529 – 2539.
[14] B. Silcox, J. Zhang, I. A. Shkrob, L. Thompson, L. Zhang, *J. Phys. Chem. C* **2019**, *123*, 16516 – 16524.
[15] G. Kwon, K. Lee, M. H. Lee, B. Lee, S. Lee, S.-K. Jung, K. Ku, J. Kim, S. Y. Park, J. E. Kwon, K. Kang, *Chem* **2019**, *5*, 2642 – 2656.
[16] C. S. Sevov, S. L. Fisher, L. T. Thompson, M. S. Sanford, *J. Am. Chem. Soc.* **2016**, *138*, 15378 – 15384.
[17] W. Duan, J. Huang, J. A. Kowalski, I. A. Shkrob, M. Vijayakumar, E. Walter, B. Pan, Z. Yang, J. D. Milshtein, B. Li, C. Liao, Z. Zhang, W. Wang, J. Liu, J. S. Moore, F. R. Brushett, L. Zhang, X. Wei, *ACS Energy Lett.* **2017**, *2*, 1156 – 1161.
[18] J. Huang, L. Cheng, R. S. Assary, P. Wang, Z. Xue, A. K. Burrell, L. A. Curtiss, L. Zhang, *Adv. Energy Mater.* **2015**, *5*, 1401782.
[19] C. Zhang, Y. Qian, Y. Ding, L. Zhang, X. Guo, Y. Zhao, G. Yu, *Angew. Chem. Int. Ed.* **2019**, *58*, 7045 – 7050; *Angew. Chem.* **2019**, *131*, 7119 – 7124.
[20] C. Zhang, Z. Niu, Y. Ding, L. Zhang, Y. Zhou, X. Guo, X. Zhang, Y. Zhao, G. Yu, *Chem* **2018**, *4*, 2814 – 2825.
[21] K. H. Hendriks, C. S. Sevov, M. E. Cook, M. S. Sanford, *ACS Energy Lett.* **2017**, *2*, 2430 – 2435.
[22] B. Hu, T. L. Liu, *J. Energy Chem.* **2018**, *27*, 1326 – 1332.
[23] J. Chai, A. Lashgari, X. Wang, C. K. Williams, J. "Jimmy" Jiang, *J. Mater. Chem. A* **2020**, *8*, 15715 – 15724.
[24] T. P. Vaid, M. S. Sanford, *Chem. Commun.* **2019**, *55*, 11037 – 11040.
[25] L. Zhang, Y. Qian, R. Feng, Y. Ding, X. Zu, C. Zhang, X. Guo, W. Wang, G. Yu, *Nat. Commun.* **2020**, *11*, 3843.
[26] J. D. Milshtein, A. P. Kaur, M. D. Casselman, J. A. Kowalski, S. Modekrutti, P. L. Zhang, N. Harsha Attanayake, C. F. Elliott, S. R. Parkin, C. Risko, F. R. Brushett, S. A. Odom, *Energy Environ. Sci.* **2016**, *9*, 3531 – 3543.
[27] A. P. Kaur, O. C. Harris, N. H. Attanayake, Z. Liang, S. R. Parkin, M. H. Tang, S. A. Odom, *Chem. Mater.* **2020**, *32*, 3007 – 3017.
[28] N. H. Attanayake, J. A. Kowalski, K. V. Greco, M. D. Casselman, J. D. Milshtein, S. J. Chapman, S. R. Parkin, F. R. Brushett, S. A. Odom, *Chem. Mater.* **2019**, *31*, 4353 – 4363.
[29] S. Ergun, C. F. Elliott, A. Preet Kaur, S. R. Parkin, S. A. Odom, *Chem. Commun.* **2014**, *50*, 5339 – 5341.
[30] A. Preet Kaur, S. Ergun, C. F. Elliott, S. A. Odom, *J. Mater. Chem. A* **2014**, *2*, 18190 – 18193.
[31] C. F. Elliott, K. E. Fraser, S. A. Odom, C. Risko, *J. Phys. Chem. A* **2021**, *125*, 272 – 278.
[32] N. Harsha Attanayake, Z. Liang, Y. Wang, A. Preet Kaur, S. R. Parkin, J. K. Mobley, R. H. Ewoldt, J. Landon, S. A. Odom, *Mater. Adv.* **2021**, *2*, 1390 – 1401.
[33] Y. Yan, S. G. Robinson, T. P. Vaid, M. S. Sigman, M. S. Sanford, *J. Am. Chem. Soc.* **2021**, https://doi.org/10.1021/jacs.1c07237.
[34] M. Park, J. Ryu, W. Wang, J. Cho, *Nat. Rev. Mater.* **2016**, *2*, 1 – 18.
[35] C. S. Sevov, S. K. Samaroo, M. S. Sanford, *Adv. Energy Mater.* **2017**, *7*, 1602027.
[36] S. G. Robinson, Y. Yan, K. H. Hendriks, M. S. Sanford, M. S. Sigman, *J. Am. Chem. Soc.* **2019**, *141*, 10171 – 10176.
[37] Y. Yan, S. G. Robinson, M. S. Sigman, M. S. Sanford, *J. Am. Chem. Soc.* **2019**, *141*, 15301 – 15306.
[38] K. H. Hendriks, S. G. Robinson, M. N. Braten, C. S. Sevov, B. A. Helms, M. S. Sigman, S. D. Minteer, M. S. Sanford, *ACS Cent. Sci.* **2018**, *4*, 189 – 196.
[39] M. Kuroboshi, T. Yamamoto, H. Tanaka, *Synlett* **2013**, *24*, 197 – 200.
[40] J. Chai, A. Lashgari, Z. Cao, C. K. Williams, X. Wang, J. Dong, J. "Jimmy" Jiang, *ACS Appl. Mater. Interfaces* **2020**, *12*, 15262 – 15270.
[41] The **4-DMPP** cycling data shows an uptick in discharge capacity at ≈40 cycles, which was observed across two repeats of this experiment (see Figure S11). This may be due to cell equilibration, but we do not have a complete explanation at this time.
[42] H. Huang, Z. M. Strater, M. Rauch, J. Shee, T. J. Sisto, C. Nuckolls, T. H. Lambert, *Angew. Chem. Int. Ed.* **2019**, *58*, 13318 – 13322; *Angew. Chem.* **2019**, *131*, 13452 – 13456.
[43] K. Gong, Q. Fang, S. Gu, S. F. Y. Li, Y. Yan, *Energy Environ. Sci.* **2015**, *8*, 3515 – 3530.
[44] X. Wei, L. Cosimbescu, W. Xu, J. Z. Hu, M. Vijayakumar, J. Feng, M. Y. Hu, X. Deng, J. Xiao, J. Liu, V. Sprenkle, W. Wang, *Adv. Energy Mater.* **2015**, *5*, 1400678.
[45] X. Wei, W. Duan, J. Huang, L. Zhang, B. Li, D. Reed, W. Xu, V. Sprenkle, W. Wang, *ACS Energy Lett.* **2016**, *1*, 705 – 711.
[46] R. S. Nicholson, *Anal. Chem.* **1965**, *37*, 1351 – 1355.
[47] While the maximum solubility of **4-DMPP**$^{++}$ is 0.45 M (electron concentration = 0.9 M) in 0.5 M $TBAPF_6$/MeCN, the symmetrical battery setup also requires the addition of 0.6 M of **5** to the electrolyte solution. To minimize the impact of the viologen on the **4-DMPP** solubility (related to the common ion effect) and to minimize the viscosity of the resulting solution, we chose to use 0.3 M **4-DMPP** (0.6 M electron concentration) in this experiment.
[48] Since this battery runs for a relatively long time (> 266 hours), the solvent slowly evaporates and bubbles develop in the battery system, disturbing the charging and discharging process and thus causing fluctuations in efficiency.

Manuscript received: September 2, 2021
Accepted manuscript online: October 20, 2021
Version of record online: November 22, 2021

